



1 Landslide susceptibility assessment of the part of the North Anatolian Fault Zone 2 (Turkey) by GIS-based frequency ratio and index of entropy models

Gökhan Demir¹

¹Department of Civil Engineering, Faculty of Engineering, Ondokuz Mayıs University, Samsun, Turkey

Correspondence: gokhan.demir@omu.edu.tr

Abstract: In the present study, landslide susceptibility assessment for the part of the North Anatolian Fault Zone is made using index of entropy models within geographical information system. At first, the landslide inventory map was prepared in the study area using earlier reports, aerial photographs and multiple field surveys. 63 cases (69 %) out of 91 detected landslides were randomly selected for modeling, and the remaining 28 (31 %) cases were used for the model validation. The landslide-trigerring factors, including slope degree, aspect, elevation, distance to faults, distance to streams, distance to road. Subsequently, landslide susceptibility maps were produced using frequency ratio and index of entropy models. For verification, the receiver operating characteristic (ROC) curves were drawn and the areas under the curve (AUC) calculated. The verification results showed that frequency ratio model (AUC=75.71%) performed slightly better than index of entropy (AUC=75.43%) model. The interpretation of the susceptibility map indicated that distance to streams, distance to road and slope degree play major roles in landslide occurrence and distribution in the study area. The landslide susceptibility maps produced from this study could assist planners and engineers for reorganizing and planning of future road construction.

Keywords: Landslide susceptibility, GIS, Nort Anatolian Fault Zone, Index of Entropy, Resadiye, Tokat.

1 Introduction

30 **1. Introduction**

31 Among various natural hazards, landslides are the most widespread and damaging.
 32 Potentials landslide-prone areas should, therefore, are identified in advance in order to
 33 reduce such damage. In this respect, landslide susceptibility assessment can provide
 34 valuable information essential for hazard mitigation through proper project planning
 35 and implementation. The main goal of landslide susceptibility analysis is to identify
 36 dangerous and high risk areas and thus landslide damage can be reduced through
 37 suitable mitigation measures (Solaimani *et al.* 2013). Different methods to prepare
 38 landslide susceptibility and hazard maps using statistical methods and GIS tools were
 39 developed in the last decade (Van Westen *et al.* 2003; Guzzetti *et al.* 2005). Many of
 40 these studies have applied statistical models such as logistic regression(Akgun 2012;
 41 Ozdemir and Altural 2013; Solaimani *et al.* 2013;Demir *et al.* 2015), bivariate(Bednarik
 42 *et al.* 2010; Pareek *et al.* 2010; Pradhan and Youssef 2010) and multivariate (Pradhan
 43 2010a, b; Choi *et al.* 2012). Probabilistic models such as frequency ratio (FR), weight of
 44 evidence (WOE), etc. have been used in landslide susceptibility mapping (Akgun *et al.*
 45 2008; Oh *et al.* 2012; Yilmaz and Keskin 2009; Youssef *et al.* 2009, 2013; Pradhan and
 46 Youssef 2010; Pradhan *et al.* 2011; Akgun *et al.* 2012; Saponaro *et al.* 2014; Sujatha *et*
 47 *al.* 2014; Demir *et al.* 2015, Bourenane *et al.* 2016, Chen *et al.* 2016b). Other different
 48 methods such as, analytical hierarchy process (AHP) (Yalcin *et al.* 2011; Pourghasemi



49 et al. 2012a; Park et al. 2013, Demir et al. 2013, Myronidis et al. 2016, Wu et al. 2016,
50 Chen et al. 2016a), index of entropy (IOE) model(Mihaela et al.2011; Devkota et al.
51 2013, Jaafari et al 2013, Youssef et al. 2015, Wang et al. 2016), certainty factor (CF) model
52 (Devkota et al. 2013), artificial neural network model (Chauhan et al. 2010; Pouydal et
53 al. 2010; Pradhan and Buchroithner 2010; Park et al. 2013),, spatial multicriteria
54 decision analysis (MCDA) approach (Akgun and Turk 2010; Akgun 2012), fuzzy logic
55 and neuro-fuzzy (Vahidnia et al. 2010; Sezer et al. 2011), decision-tree methods
56 (Nefeslioglu et al. 2010; Pradhan 2013), fuzzy logic (Pourghasemi et al. 2012a, 2012b,
57 2012c; Sharma et al. 2013), support vector machine (SVM) (Yilmaz 2010; Pradhan
58 2013) have also been employed for the purpose of landslide susceptibility mapping.
59 This study aims to develop landslide susceptibility maps of the part of the North
60 Anatolian Fault Zone, southeast Resadiye-Koyulhisar Turkey, (Fig. 1), using index of
61 entropy (IOE) model. To achieve this, index of entropy analysis methodology, to obtain
62 landslide susceptibility map using the geographic information system was developed,
63 applied, and verified in the study area.



64

65

Figure 1. Study Area

66

67 **2. Study area**

68 The study area is located in the the North Anatolian Fault Zone, between the southeast
69 Resadiye to Koyulhisar Sivas province. The area lies between $44^{\circ}70'64''$ and $44^{\circ}56'84''$ latitude and $36^{\circ}21'87''$ and $41^{\circ}47'09''$ longitude, and covers an area about of
70 720 km².

72 According to a geological map prepared by General Directory of Mineral Research and
73 Exploration, north of the NAFZ there are, from old to young, Upper Cretaceous-age
74 volcanic and sedimentary units, Maastrichtian-age limestone, and Pliocene-age basalt

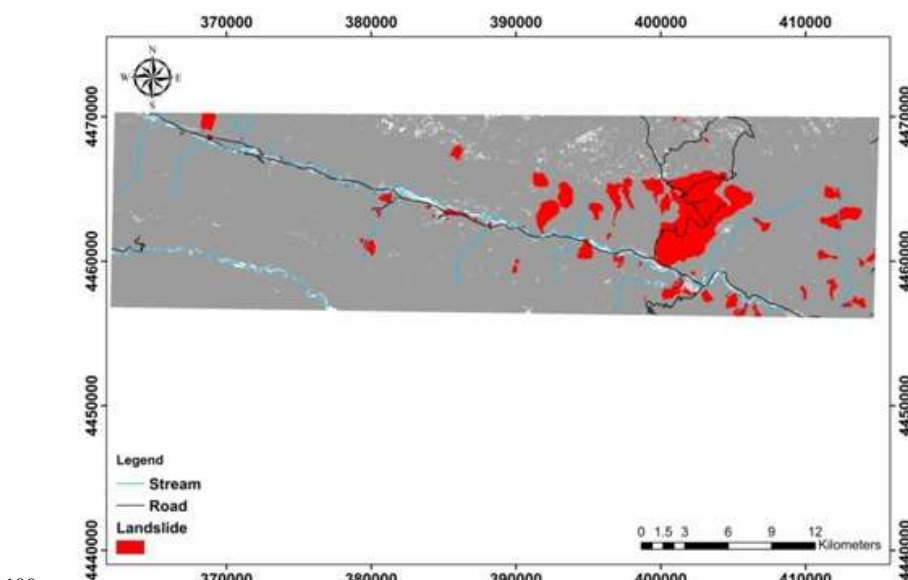


75 and other volcanic units. While the Upper Cretaceous volcanic and sedimentary units on
76 the lower slopes have a gentle slope morphology, Maastrichtian limestones present a
77 very steep morphology. While the dip of the lower beds of the limestone varies over
78 short distances due to the effect of the NAFZ, it is generally to the northeast (Gokceoglu
79 et al. 2005). Landslides are common natural hazards in the seismically active North
80 Anatolian Fault Zone (NAFZ), which is 1,100 km in length and is moving westward
81 with the rate of 2.5 cm every year according to geological and GPS data (Demir et al
82 2013). The latest catastrophic event occurred on March 17, 2005 at Kuzulu (Sivas) in the
83 valley. The landslide was initiated within highly weathered volcanics in the mode of
84 sliding and then transformed to an earth flow. It killed 15 people, and more than 30
85 houses and a mosque were buried and damaged by the earth flow material. A second but
86 smaller landslide originated from the same source areas after 4 days and caused
87 additional damages (Gokceoglu et al. 2005; Ulusay et al. 2007; Yilmaz 2009). After the
88 main event, the governor needed landslide susceptibility maps of the landslide area.

89 **3. Data production**

90 The study began with the preparation of a landslide inventory map based on field work,
91 earlier reports and satellite images. Landslide inventory maps show the areal
92 distribution of existing landslide areas and their characteristics. These maps indicate the
93 landslides, which are perceptible on site (Cevik and Topal 2003). In total, 321
94 landslides were mapped (Fig. 2) and subsequently digitized for further analysis. The
95 mapped landslides cover an area of 47.81 km², which constitutes 6.68 % of the entire
96 study area. From these landslides, 63 (69 %) randomly selected instabilities were taken
97 for making landslide susceptibility models and 28 (31 %) were used for validating the
98 models.

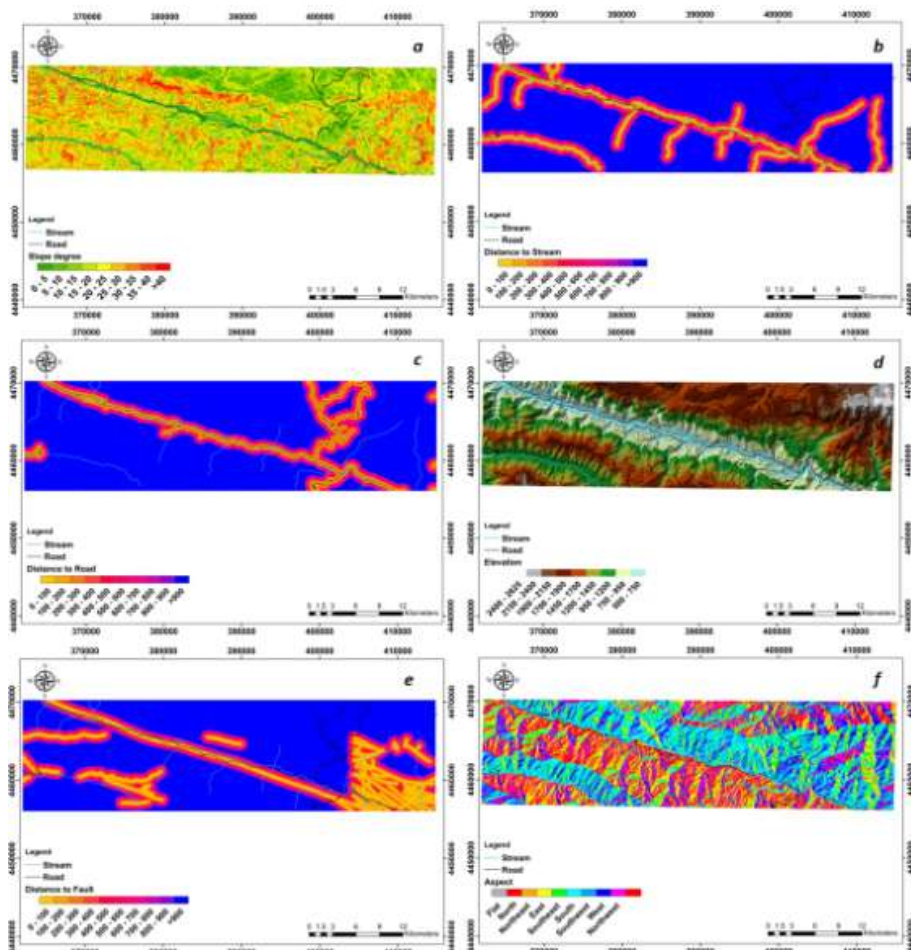
99



100
101 **Figure 2.** Landslide inventory map
102



103 The number of landslide-conditioning factors may range from only a few numbers to
104 several (Mohammady et al. 2012; Pourghasemi et al. 2012d; Papathanassiou et al.
105 2012). The selection of these factors mainly depends on the availability of data for the
106 study area and the relevance with respect to landslide occurrences (Papathanassiou et
107 al. 2012). According to the Ayalew and Yamagishi (2005), in GIS-based studies, the
108 selected factors should be operational, complete, non-uniform, measurable, and non-
109 redundant. We prepared six thematic data layers representing the following landslide
110 conditioning factors: slope degree, aspect, elevation, distance to faults, distance to
111 streams, distance to road (Figure 3).
112



113
114 **Figure 3.** Conditioning Factors(a.slope degree, b.distance to stream, c.distance to road,
115 d.elevation, e.distance to faults,f.aspect.)



116 The main parameter of the slope stability analysis is the slope degree(S. Lee and K. Min
117 2001). Because the slope degree is directly related to the landslides, it is frequently used
118 in preparing landslide susceptibility maps[S. Lee, J. H. Ryu, J. S. Won and H. J. Park
119 (2004), M. Ercanoglu, C. Gokceoglu, T. W. J. Van Asch (2004, A. Clerici, S. Perego, C.
120 Tellini and P. Vescovi (2002) . For this reason, the slope degree map of the study area is
121 prepared from the digital elevation model (DEM) and divided into nine slope classes
122 with an interval of 5°(Figure 3). Aspect and elevation also were extracted from the
123 DEM. Aspects are grouped into 9 classes such as flat (-1), north (337.5°–360°, 0°–
124 22.5°), northeast (22.5°–67.5°), east (67.5°–112.5°), southeast (112.5°–157.5°), south
125 (157.5°–202.5°), southwest (202.5°–247.5°), west (247.5°–292.5°), and northwest
126 (292.5°–337.5°).In the study area, the elevation ranges between 500 and 2,625 m. The
127 elevation values were divided into nine classes (Figure 3). The distance from faults,
128 road and stream is calculated at 100m intervals using the geological map (Figure 9). An
129 important parameter that controls the stability of a slope is the saturation degree of the
130 material on the slope(Yalçın 2008, Yalçın and Bulut 2007). The closeness of the slope
131 to drainage structures is another important factor in terms of stability. Streams may
132 adversely affect stability by eroding the slopes or by saturating the lower part of
133 material resulting in water level increases(Pourghasemi et al. 2012a, Gökçeoglu 1996,
134 Saha et al. 2002). For this reason, ten different buffer zones were created within the
135 study area to determine the degree to which the streams affected the slopes. A road
136 constructed can cause a disturbance of the slopes that lead to increase in stress on the
137 back of the slope, because of changes in topography and decrease of load on toe, some
138 tension cracks may develop. Although a slope is balanced before the road construction,
139 some instability may be happened because of negative effects of excavation. In the
140 current study many landslides were recorded along the roads in the study area that is
141 due to road construction. The distance from roads was calculated and reclassified into
142 ten classes.

143 **4. Landslide Susceptibility Analysis**

144 **a. Application of Index of Entropy Model**

145 In this study index of entropy model was used for landslide susceptibility analysis using
146 six landslide conditioning factors.

147 The entropy indicates the extent of the instability, disorder, imbalance, and uncertainty
148 of a system (Yufeng and Fengxiang, 2009). The entropy of a landslide refers to the
149 extent that various factors influence the development of a landslide (Pourghasemi et al.,
150 2012b; Jaafari et al., 2013). Several important factors provide additional entropy into
151 the index system. Therefore, the entropy value can be used to calculate objective
152 weights of the index system. The equations used to calculate the information coefficient
153 W_j representing the weight value for the parameter as a whole (Bednarik et al., 2010;
154 Constantin et al., 2011) are given as follows:
155



$$P_{ij} = \frac{b}{a} \quad (1)$$

$$(P_{ij}) = \frac{P_{ij}}{\sum_{j=1}^{S_j} P_{ij}} \quad (2)$$

$$H_j = -\sum_{i=1}^{S_j} (P_{ij}) \log_2 (P_{ij}), j = 1, \dots, n \quad (3)$$

$$H_{j \max} = \log_2 S_j - \text{number of classes} \quad (4)$$

$$I_j = \frac{H_{j \max} - H_j}{H_{j \max}}, I = (0,1), j = 1, \dots, n \quad (5)$$

$$W_j = I_j P_{ij} \quad (6)$$

157

158 where a and b are the domain and landslide percentages, respectively, (P_{ij}) is the
 159 probability density, H_j and $H_{j \max}$ represent entropy values, I_j is the information
 160 coefficient and W_j represents the resultant weight value for the parameter as a whole.

161 The final landslide susceptibility map was prepared by the summation of weighted
 162 products of the secondarily parametric maps. The final landslide susceptibility maps
 163 using index of entropy model was developed using the following equation:

164

$$Y_{iE} = ((Slope \ deg \ ree * 0,110) + (Aspect * 0,080) + \\ (Elevation * 0,136) + (Distance \ to \ Road * 0,023) + \\ (Distance \ to \ Stream * 0,023) + (Distance \ to \ Fault) * 0,005) \quad (7)$$

166

167 where Y is the value of landslide susceptibility (Fig. 4). The result of this summation is
 168 a continuous interval of values from 0.7297 to 6.1861, which represents the landslide
 169 susceptibility index. A natural break classification method was used to divide the
 170 interval into four classes and a susceptibility map was prepared (Bednarik et al., 2010;
 171 Constantin et al., 2011; Erner et al., 2010; Falaschi et al., 2009; Ram Mohan et al.,
 172 2011; Xu et al., 2012a, 2012b). According to the landslide susceptibility map generated
 173 with the IOE model (Fig. 4 and Table 1), it was found that 24.87% and 23.50% of the
 174 total landslides falls in the very low and low susceptibility zones respectively.
 175 Moderate, high, and very high susceptible zones represent 20.37%, 16.42%, and
 176 14.83% of the landslides pixels, respectively.

177

178 **Table 1** Spatial relationship between each landslide conditioning factor and landslides
 179 using index of entropy model.

Factor (Parameter)	Class	Percentage of pixels in the class (%) (a)	Percentage of landslide pixels(%) (b)	Pij	(Pij)	Hj	Hjmax	Ij	Wj
Elevation (m)	500-750	11.324	10.406	0.919	0.147	2.551	3.170	0,195	0,136
	750-950	13.048	16.226	1.244	0.199				
	950-1200	18.265	21.566	1.181	0.189				
	1200-1450	18.478	24.770	1.341	0.214				
	1450-1700	19.762	20.921	1.059	0.169				

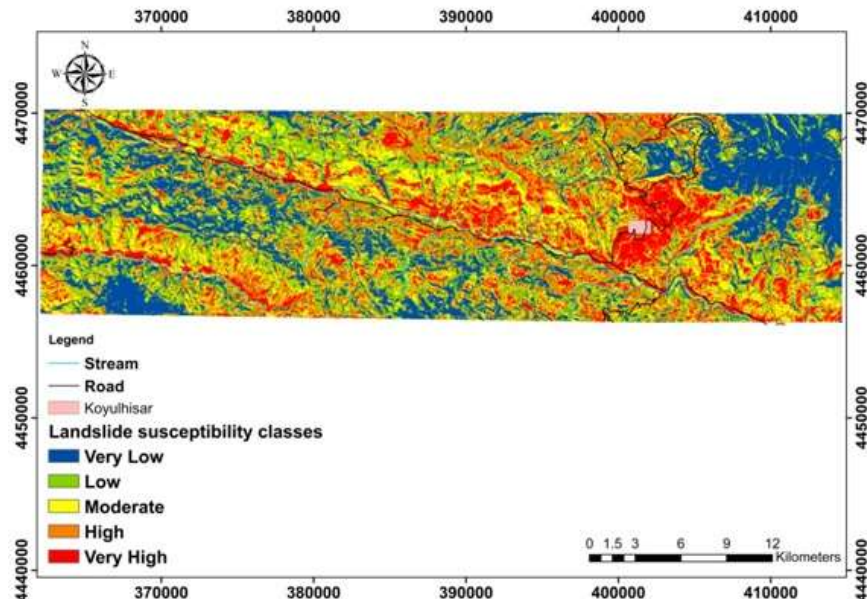


1700-1900	12.213	6.021	0.493	0.079				
1900-2150	4.096	0.091	0.022	0.004				
2150-2400	2.115	0.000	0.000	0.000				
2400-2625	0.699	0.000	0.000	0.000				
Slope degree (°)					2.770	3.170	0.126	0,110
0-5	7.093	7.888	1.112	0.142				
5-10	11.692	24.212	2.071	0.265				
10-15	15.430	26.660	1.728	0.221				
15-20	16.929	17.950	1.060	0.136				
20-25	16.714	11.004	0.658	0.084				
25-30	15.076	6.438	0.427	0.055				
30-35	10.864	4.399	0.405	0.052				
35-40	4.870	1.338	0.275	0.035				
>40	1.331	0.111	0.083	0.011				
Aspect	FLAT	1.043	0.302	0.290	0.034	2.871	3.170	0,094
	NORTH	13.922	5.270	0.378	0.045			0,080
	NORTHEA ST	12.046	4.593	0.381	0.045			
	EAST	9.461	5.779	0.611	0.072			
	SOUTHEAS T	10.956	11.476	1.047	0.124			
	SOUTH	15.267	25.409	1.664	0.196			
	SOUTHWE ST	13.818	24.351	1.762	0.208			
	WEST	11.493	15.909	1.384	0.163			
	NORTHWE ST	11.994	6.911	0.576	0.068			
Distance to Stream (m)	0-100	3.692	7.789	2.110	0.152	3.266	3.322	0,017
	100-200	3.630	7.086	1.952	0.140			
	200-300	3.584	5.757	1.606	0.115			
	300-400	3.614	5.274	1.459	0.105			
	400-500	3.522	4.877	1.384	0.100			
	500-600	3.440	4.510	1.311	0.094			
	600-700	3.307	3.666	1.108	0.080			
	700-800	3.133	3.451	1.101	0.079			
	800-900	3.110	3.400	1.093	0.079			
	>900	68.968	54.190	0.786	0.056			
Distance to Road (m)	0-100	6.937	12.505	1.803	0.142	3.262	3.322	0,018
	100-200	6.445	10.563	1.639	0.130			
	200-300	6.258	9.866	1.577	0.125			
	300-400	6.179	9.075	1.469	0.116			
	400-500	5.825	7.848	1.347	0.106			
	500-600	5.016	5.799	1.156	0.091			
	600-700	5.813	6.422	1.105	0.087			
	700-800	5.801	5.880	1.014	0.080			
	800-900	6.566	6.414	0.977	0.077			
	>900	45.159	25.628	0.568	0.045			
Distance to	0-100	6.331	4.788	0.756	0.079	3.305	3.322	0,005
								0,005



Fault (m)					
100-200	5.193	4.444	0.856	0.090	
200-300	4.245	3.980	0.938	0.098	
300-400	3.682	3.346	0.909	0.095	
400-500	3.261	3.676	1.127	0.118	
500-600	2.940	3.592	1.222	0.128	
600-700	2.984	3.167	1.061	0.111	
700-800	2.899	2.548	0.879	0.092	
800-900	2.805	2.153	0.768	0.080	
>900	65.660	68.306	1.040	0.109	

180



181
 182

183 **Figure 4.** Landslide susceptibility map IOE

184
 185

b. Application of Frequency ratio method

186 Frequency ratio method is a simple and understandable probabilistic model, and the
 187 model is based on the observed relationships between distribution of landslides and
 188 each landslide-causative factor, to reveal the correlation between landslide locations and
 189 the factors in the study area (Lee and Pradhan, 2007). To calculate the frequency ratio,
 190 the ratio of landslide occurrence to non-occurrence (Regmi et al., 2013) was calculated
 191 for each factor's class. Therefore, the frequency ratio for each factor's class was
 192 calculated from its relationship with landslide events. The frequency ratio is defined as
 193 shown in Equation (8).

194

$$195 \quad FR = \frac{PLO}{PIF} \quad (8)$$

196



197 Here, PLO is the subcategory percentage of each factor conditioning landslide in a
 198 landslide area, while PIF is the category percentage of each factor conditioning
 199 landslide (Table 2).

200 **Table.2** Frequency ratio values of the landslide-trigerring parameters.

Factor (Parameter)	Class	Number of pixels in class	Percentage of pixels in the class (%) (a)	Number of landslide pixels	Percentage of landslide pixels(%) (b)	FREQUENCY RATIO (FR) (b/a)
Elevation (m)	500-750	130386	11.324	5166	10.406	0.919
	750-950	150242	13.048	8055	16.226	1.244
	950-1200	210313	18.265	10706	21.566	1.181
	1200-1450	212763	18.478	12297	24.770	1.341
	1450-1700	227550	19.762	10386	20.921	1.059
	1700-1900	140627	12.213	2989	6.021	0.493
	1900-2150	47161	4.096	45	0.091	0.022
	2150-2400	24348	2.115	0	0.000	0.000
	2400-2625	8044	0.699	0	0.000	0.000
Slope degree (°)	0-5	81676	7.093	3916	7.888	1.112
	5-10	134628	11.692	12020	24.212	2.071
	10-15	177671	15.430	13235	26.660	1.728
	15-20	194923	16.929	8911	17.950	1.060
	20-25	192448	16.714	5463	11.004	0.658
	25-30	173594	15.076	3196	6.438	0.427
	30-35	125095	10.864	2184	4.399	0.405
	35-40	56076	4.870	664	1.338	0.275
	>40	15323	1.331	55	0.111	0.083
Aspect	FLAT	12005	1.043	150	0.302	0.290
	NORTH	160305	13.922	2616	5.270	0.378
	NORTHEAST	138703	12.046	2280	4.593	0.381
	EAST	108940	9.461	2869	5.779	0.611
	SOUTHEAST	126147	10.956	5697	11.476	1.047
	SOUTH	175786	15.267	12614	25.409	1.664
	SOUTHWEST	159110	13.818	12089	24.351	1.762
	WEST	132340	11.493	7898	15.909	1.384
	NORTHWEST	138098	11.994	3431	6.911	0.576
Distance to Stream (m)	0-100	42513	3.692	3867	7.789	2.110
	100-200	41798	3.630	3518	7.086	1.952
	200-300	41271	3.584	2858	5.757	1.606
	300-400	41614	3.614	2618	5.274	1.459
	400-500	40558	3.522	2421	4.877	1.384
	500-600	39604	3.440	2239	4.510	1.311
	600-700	38082	3.307	1820	3.666	1.108
	700-800	36070	3.133	1713	3.451	1.101
	800-900	35807	3.110	1688	3.400	1.093
	>900	794117	68.968	26902	54.190	0.786
Distance to Road (m)	0-100	79875	6.937	6208	12.505	1.803



100-200	74209	6.445	5244	10.563	1.639
200-300	72053	6.258	4898	9.866	1.577
300-400	71146	6.179	4505	9.075	1.469
400-500	67076	5.825	3896	7.848	1.347
500-600	57759	5.016	2879	5.799	1.156
600-700	66937	5.813	3188	6.422	1.105
700-800	66800	5.801	2919	5.880	1.014
800-900	75608	6.566	3184	6.414	0.977
>900	519971	45.159	12723	25.628	0.568
Distance to Fault (m)	0-100	72894	6.331	2377	4.788
	100-200	59789	5.193	2206	4.444
	200-300	48884	4.245	1976	3.980
	300-400	42392	3.682	1661	3.346
	400-500	37545	3.261	1825	3.676
	500-600	33854	2.940	1783	3.592
	600-700	34362	2.984	1572	3.167
	700-800	33376	2.899	1265	2.548
	800-900	32301	2.805	1069	2.153
	>900	756037	65.660	33910	68.306
					1.040

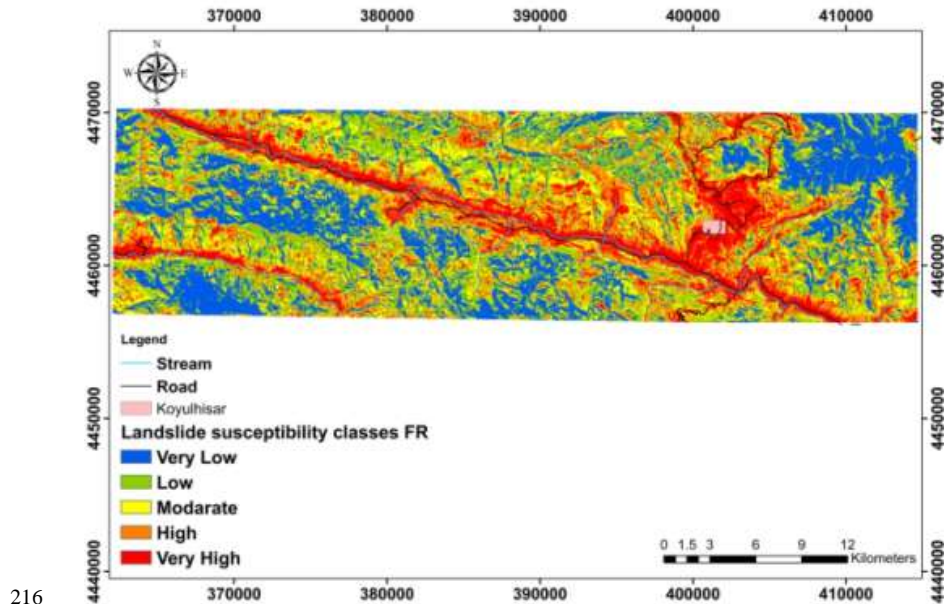
201

202 Therefore, the greater the ratio above unity, the stronger the relationship between
 203 landslide occurrence and the given factor's class attribute, and the lower the ratio below
 204 unity, the lesser the relationship between landslide occurrence and the given factor's
 205 class attribute (Lee and Pradhan, 2006; Yalcin et al., 2011). To calculate the landslide
 206 susceptibility index (LSI), each factor's frequency ratio values were summed as shown
 207 in Equation 9.

208
$$LSI = \sum_{i=1}^n FR \quad (9)$$

209

210 The LSI map was reclassified using the equal interval method in GIS, and as a result,
 211 the study area was divided into five susceptibility classes: very low, low, moderate high,
 212 and very high (Fig. 5). According to this landslide susceptibility map, 24.67 % of the
 213 total area was determined to be very low susceptible. Low, moderate, and high
 214 susceptible zones constitute 23.08 %, 19.70 %, and 16.85 % of the area, respectively.
 215 The very high susceptible area is 15.69 % of the total area.



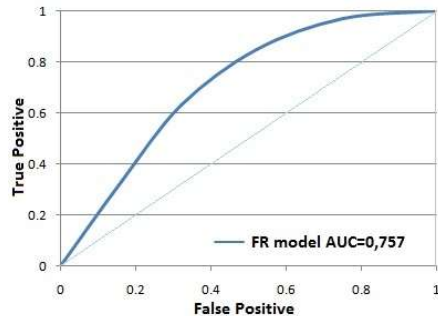
216
217 **Figure 5.** Landslide susceptibility map FR
218
219

5. Validation of Landslide Susceptibility map

220 Landslide susceptibility maps without validation are less meaningful (Chung and Fabbri
221 1998). In the current study, validation of the landslides susceptibility maps was checked
222 by using receiver operating characteristics (ROC) (Akgun et al., 2012; Tien Bui et al.,
223 2012a, b, 2013; Regmi et al., 2014; Ozdemir and Altural, 2013). The ROC curve is a
224 useful method for representing the quality of deterministic and probabilistic detection
225 and forecast systems. The ROC plots the different accuracy values obtained against the
226 whole range of possible threshold values of the functions, and the ROC serves as a
227 global accuracy statistic for the model, regardless of a specific discriminant threshold
228 (Pourghasemi et al., 2012). In the ROC curve, the sensitivity of the model (the
229 percentage of existing landslide pixels correctly predicted by the model) is plotted
230 against 1-specificity (the percentage of predicted landslide pixels over the total study
231 area) (Mohammady et al., 2012; Jaafari et al., 2013). The area under the ROC curve
232 (AUC) represents the quality of the probabilistic model to reliably predict the
233 occurrence or non-occurrence of landslides. A good fit model has an AUC values range
234 from 0.5–1, while values below 0.5 represent a random fit. The success rate results were
235 obtained by comparing the landslide training data with the susceptibility maps (Fig. 6).
236 AUC plot assessment results showed that the AUC values were 0.7571 and 0.7543 for
237 FR and IOE models and the training accuracy were 75.71 and 75.43 %, respectively.
238 From the results of the AUC evaluation, it is seen that both the success rate curve show
239 almost similar result. All the models employed in this study showed reasonably good
240 accuracy in predicting the landslide susceptibility of the study area.



241



242

243

244

245

246

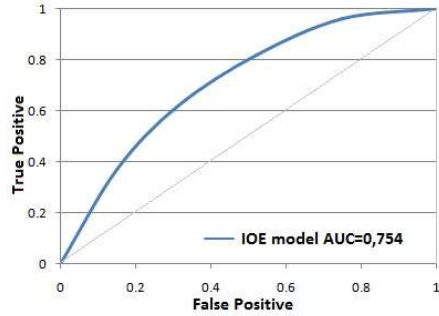


Figure 6. Success rate curves of FR and IOE models of the study area.

6. Conclusion

In this study, the accepted models, frequency ratio and index of entropy, within a GIS environment for the aim of LSM have been used. For this purpose, six triggering factors, i.e., slope degree, aspect, elevation, distance to faults, distance to streams and distance to road were used. A total of 91 landslides were identified and mapped. Out of which, 63 (69 %) were randomly selected for generating a model and the remaining 28 (31 %) were used for validation purposes. In this study, five landslide susceptibility classes, i.e., very low, low, moderate, high, and very high susceptibility for landsliding, were derived with equal interval method. The validation has been determined by using the ROC method in which the accuracy of the LS maps produced by the frequency ratio and index of entropy models was 0.757 and 0.754, respectively for success rate technique. This shows that all the models employed in this study showed reasonably good accuracy in predicting the landslide susceptibility of the part of the North Anatolian Fault Zone (Turkey). All susceptibility zones require further engineering geological and geotechnical considerations. The increasing population pressure has forced people to concentrate their activities on steep mountain slopes. Thus, to safeguard the life and property from landslides, the susceptibility map can be used as basic tools in land management and planning future construction projects in this area. The landslide susceptibility map produced in this study can be used for optimum management by decision makers and land use planners, and also avoidance of susceptible regions in study area.

7. References

Akgun, A., (2012). A comparison of landslide susceptibility maps produced by logistic regression, multi-criteria decision, and likelihood ratio methods: a case study at Izmir, Turkey. *Landslides* 9 (1), 93–106. <http://dx.doi.org/10.1007/s10346-011-0283-7>.

Akgun A, Turk N. (2010). Landslide susceptibility mapping for Ayvalik (Western Turkey) and its vicinity by multi-criteria decision analysis. *Environmental Earth Science*; 61(3): 595-611



276 Akgun, A., Sezer, E.A., Nefeslioglu, H.A., Gokceoglu, C., and Pradhan, B., (2012). An
277 easy-to-use MATLAB program (MamLand) for the assessment of landslide
278 susceptibility using a Mamdani fuzzy algorithm. *Computers & Geosciences*, 38, 23–34

279 Akgün, A., Dag, S., Bulut, F., (2008). Landslide susceptibility mapping for a
280 landslide-prone area (Findikli, NE of Turkey) by likelihood-frequency ratio and
281 weighted linear combination models. *Environmental Geology* 54, 1127–1143.

282 Ayalew, L. and Yamagishi, H., (2005). The application of GIS-based logistic regression
283 for landslide susceptibility mapping in the Kakuda-Yahiko mountains, Central Japan.
284 *Geomorphology*, 65, 15–31.

285 Bednarik, M., Magulová, B., Matys, M., Marschalko, M., (2010). Landslide
286 susceptibility assessment of the Kral'ovany–Liptovsky' Mikuláš railway case study.
287 *Physics and Chemistry of the Earth* 35, 162–171.

288 Bourenane H., Guettouche M. S., Bouhadad Y., Braham M., 2016. Landslide hazard
289 mapping in the Constantine city, Northeast Algeria using frequency ratio, weighting
290 factor, logistic regression, weights of evidence, and analytical hierarchy process
291 methods. *Arab J Geosci* (2016) 9: 154 DOI 10.1007/s12517-015-2222-8

292 Cevik, E. and Topal, T., (2003). GIS-based landslide susceptibility mapping for a
293 problematic segment of the natural gas pipeline, Hendek (Turkey). *Environmental
294 Geology*, 44, 949–962.

295 Chauhan, S., Sharma, M., Arora, M.K., Gupta, N.K., (2010). Landslide susceptibility
296 zonation
297 through ratings derived from artificial neural network. *International Journal of Applied
298 Earth Observation and Geoinformation* 12, 340–350.

299 Choi J, Oh HJ, Lee HJ, Lee C, Lee S (2012). Combining landslide susceptibility maps
300 obtained from frequency ratio, logistic regression, and artificial neural network models
301 using ASTER images and GIS. *Eng Geol* 124:12–23

302 Clerici A, Perego S, Tellini C, Vescovi P (2002). A procedure for landslide
303 susceptibility zonation by the conditional analysis method. *Geomorphology* 48:349–364

304 Constantin, M., Bednarik, M., Jurchescu, M.C., Vlaicu, M., (2011). Landslide
305 susceptibility assessment using the bivariate statistical analysis and the index of entropy
306 in the Sibiciu Basin (Romania). *Environmental Earth Science* 63, 397–406.

307 Chen W., Li W., Chai H., Hou E., Li X., Ding X., (2016a) GIS-based landslide
308 susceptibility mapping using analytical hierarchy process (AHP) and certainty factor
309 (CF) models for the Baozhong region of Baoji City, China. *Environ Earth Sci* 75:63
310 DOI 10.1007/s12665-015-4795-7

311 Chen W., Chai H., Sun X., Wang Q., Ding X., Hong H., (2016b). A GIS-based
312 comparative study of frequency ratio, statistical index and weights-of-evidence models
313 in landslide susceptibility mapping. *Arab J Geosci* 9: 204 DOI 10.1007/s12517-015-
314 2150-7

315 Chung CJ, Fabbri AG (1998) Probabilistic prediction models for landslide hazard
316 mapping. *Photogramm Eng Rem S* 65(12):1389–1399

317

318 Demir G, Aytekin M, Akgün A, İkizler SB, & Tatar O (2013). A comparison of
319 landslide susceptibility mapping of the eastern part of the North Anatolian Fault Zone
320 (Turkey) by likelihood-frequency ratio and analytic hierarchy process methods. *Natural
321 hazards*, 65(3), 1481–1506



322 Demir, G., Aytekin, M., Akgun, A., (2015). Landslide susceptibility mapping by
323 frequency ratio and logistic regression methods: an example from Niksar–Resadiye
324 (Tokat, Turkey). *Arab. J. Geosci.* <http://dx.doi.org/10.1007/s12517-014-1332-z>.

325 Ercanoglu M, Gokceoglu C, van Asch TWJ (2004). Landslide susceptibility zoning
326 north of Yenice (NW Turkey) by multivariate statistical techniques. *Nat Hazards* 32:1–
327 23

328 Erner, A., Sebnem, H., Duzgun, B., (2010). Improvement of statistical landslide
329 susceptibility mapping by using spatial and global regression methods in the case of
330 More and Romsdal (Norway). *Landslides* 7, 55–68.

331 Falaschi, F., Giacomelli, F., Federici, P.R., Puccinelli, A., D'Amato Avanzi, G., Pochini,
332 A., Ribolini, A., (2009). Logistic regression versus artificial neural networks: landslide
333 susceptibility evaluation in a sample area of the Serchio River valley, Italy. *Natural
334 Hazards* 50, 551–569.

335 N. T. Long and D. S. Florimond (2012). Application of an analytical hierarchical
336 process approach for landslide susceptibility mapping in A Luoi district, Thua Thien
337 Hue Province, Vietnam," *Environmental Earth Science*, vol. 66, no. 7, pp. 1739-1752.

338 Gokceoglu C. and Aksoy H. (1996). Landslide susceptibility mapping of the slopes in
339 the residual soils of the Mengen region (Turkey) by deterministic stability analyses and
340 image processing techniques," *Engineering Geology*, vol. 44, no. 1-4, pp. 147-161.

341 Gokceoglu C, Sönmez H, Nefeslioglu HA, Duman TY, Can, T. (2005). The March 17,
342 2005 Kuzulu landslide (Sivas, Turkey) and landslide susceptibility map of its near
343 vicinity. *Engineering Geology*;81 (1): 65-83.

344 Guzzetti, F., Reichenbach, P., Cardinali, M., Galli, M., and Ardizzone, F., (2005).
345 Landslide hazard assessment in the Staffora basin, Northern Italian Apennines.
346 *Geomorphology*, 72, 272–299.

347 Jaafari, A., Najafi, A., Pourghasemi, H.R., Rezaeian. J., and Sattarian, A., (2013). GIS-
348 based frequency ratio and index of entropy models for landslide susceptibility
349 assessment in the Caspian forest, northern Iran. *International Journal of Environmental
350 Science and Technology*, DOI: 10.1007/s13762-013-0464-0.

351 Kannan M, Saranathan E, & Anabalagan R (2013). Landslide vulnerability mapping
352 using frequency ratio model: a geospatial approach in Bodi-Bodimettu Ghat section,
353 Theni district, Tamil Nadu, India. *Arabian journal of Geosciences*, 6(8), 2901-2913

354 Mihaela C, Martin B, Marta CJ, & Marius V (2011). Landslide susceptibility
355 assessment using the bivariate statistical analysis and the index of entropy in the Sibiciu
356 Basin (Romania). *Environ Earth Sci* 63:397-406

357 Mohammady, M., Pourghasemi, H.R., and Pradhan, B., (2012). Landslide susceptibility
358 mapping at Golestan Province Iran: a comparison between frequency ratio, Dempster-
359 Shafer, and weightsof evidence models. *Journal of Asian Earth Sciences*, 61, 221–236.

360 Myronidis D., Papageorgiou C., Theophanous S.,2016. Landslide susceptibility
361 mapping based on landslide history and analytic hierarchy process (AHP).*Nat Hazards*
362 (2016) 81:245–263 DOI 10.1007/s11069-015-2075-1

363 Oh, H.J., Park, N.W., Lee, S.S., Lee, S., (2012). Extraction of landslide-related factors
364 from ASTER imagery and its application to landslide susceptibility mapping.
365 *International Journal of Remote Sensing* 33 (10), 3211–3231.

366 Ozdemir, A. and Altural, T., (2013). A comparative study of frequency ratio, weights of
367 evidence and logistic regression methods for landslide susceptibility mapping: Sultan
368 Mountains, SW Turkey. *Journal of Asian Earth Sciences*, 64, 180–197



369 Pourghasemi HR, Pradhan B, & Gokceoglu C (2012a). Application of fuzzy logic and
370 analytical hierarchy process (AHP) to landslide susceptibility mapping at Haraz
371 watershed, Iran. *Nat Hazards* 63:965-996

372 Pourghasemi HR, Pradhan B, Gokceoglu C, & Moezzi, KD (2012b). Landslide
373 susceptibility mapping using a spatial multi criteria evaluation model at Haraz
374 Watershed, Iran. In *Terrigenous Mass Movements* (pp. 23-49). Springer Berlin
375 Heidelberg

376 Pourghasemi, H.R., Pradhan, B., Gokceoglu, C., Mohammadi, M., Moradi, H.R.,
377 (2012c). Application of weights-of-evidence and certainty factor models and their
378 comparison in landslide susceptibility mapping at Haraz watershed, Iran. *Arabian*
379 *Journal of Geosciences*. <http://dx.doi.org/10.1007/s12517-012-0532-7>.

380 Pourghasemi, H.R., Gokceoglu, C., Pradhan, B., Deylami Moezzi, K., (2012d).
381 Landslide susceptibility mapping using a spatial multi criteria evaluation model: case
382 study at Haraz Watershed, Iran. In: Pradhan, B., Buchroithner, M. (Eds.), *Terrigenous*
383 *Mass Movements*. Springer-Verlag, Berlin Heidelberg, pp. 23-49. <http://dx.doi.org/10.1007/978-3-642-25495-6-2>.

385 Pareek N, Sharma ML, & Arora MK (2010). Impact of seismic factors on landslide
386 susceptibility zonation: a case study in part of Indian Himalayas. *Landslides* 7(2):191-
387 201

388 Park, N.W., (2011). Application of Dempster-Shafer theory of evidence to GIS-based
389 landslide susceptibility analysis. *Environmental Earth Science* 62, 367-376.

390 Pouydal CP, Chang C, Oh HJ, & Lee S (2010). Landslide susceptibility maps
391 comparing frequency ratio and artificial neural networks: a case study from the Nepal
392 Himalaya. *Environ Earth Sci* 61:1049-1064

393 Pradhan, B., (2013). A comparative study on the predictive ability of the decision tree,
394 support vector machine and neuro-fuzzy models in landslide susceptibility mapping
395 using GIS. *Computers & Geosciences*, 51, 350-365.

396 Pradhan, B. and Lee, S., (2010a). Delineation of landslide hazard areas using frequency
397 ratio, logistic regression and artificial neural network model at Penang Island, Malaysia.
398 *Environmental Earth Sciences*, 60, 1037-1054

399 Pradhan, B., Lee, S., (2010b). Landslide susceptibility assessment and factor effect
400 analysis: back propagation artificial neural networks and their comparison with
401 frequency ratio and bivariate logistic regression modelling. *Environmental Modelling*
402 and *Software* 25 (6), 747-759.

403 Pradhan, B., Lee, S., Buchroithner, M.F., (2010c). Remote sensing and GIS-based
404 landslide susceptibility analysis and its cross-validation in three test areas using a
405 frequency ratio model. *Photogrammetrie Fernerkundung Geoinformation* 1, 17-32.
406 <http://dx.doi.org/10.1127/14328364/2010/0037.>

407 Pradhan, B., Mansor, S., Pirasteh, S., Buchroithner, M., (2011). Landslide hazard and
408 risk analyses at a landslide prone catchment area using statistical based geospatial
409 model. *International Journal of Remote Sensing* 32 (14), 4075-4087. <http://dx.doi.org/10.1080/01431161.2010.484433>

411 Ram Mohan, V., Jeyaseelan, A., Naveen Raj, T., Narmatha, T., Jayaprakash, M.,
412 (2011). Landslide susceptibility mapping using frequency ratio method and GIS in
413 South eastern part of Nilgiri District, Tamilnadu, India. *International Journal of*
414 *Geomatics and Geoscience* 1 (4), 951-961.

415 Regmi, A.D., Devkota, K.C., Yoshida, K., Pradhan, B., Pourghasemi, H.R., Kumamoto,
416 T., and Akgun, A., (2014). Application of frequency ratio, statistical index, and



417 weights-of-evidence models and their comparison in landslide susceptibility mapping in
418 Central Nepal Himalaya. *Arabian Journal of Geosciences*, 7, 725–742.

419 Lee S, Min K (2001) Statistical analyses of landslide susceptibility at Yongin, Korea.
420 *Environ Geol* 40:1095–1113

421 Lee S, Ryu JH, Won JS, Park HJ. (2004). Determination and application of the weights
422 for landslide susceptibility mapping using an artificial neural network, *Engineering*
423 *Geology* 2004; 71: 289–302.

424 Saha A.K., Gupta R. P. and Arora M. K. (2002). GIS-based landslide hazard zonation
425 in the Bhagirathi (Ganga) valley, Himalayas, *International Journal of Remote Sensing*,
426 vol. 23, no. 2, pp. 357–369.

427 Saponaro A, Pilz M, Wieland M, Bindi D, Moldobekov B, & Parolai S (2014).
428 Landslide susceptibility analysis in data-scarce regions: the case of Kyrgyzstan. *Bulletin*
429 of *Engineering Geology and the Environment*, 1-20.

430 Sezer, E.A., Pradhan, B., Gokceoglu, C., (2011). Manifestation of an adaptive neuro-
431 fuzzy model on landslide susceptibility mapping: Klang valley, Malaysia. *Expert*
432 *Systems with Applications* 38 (7), 8208–8219.

433 Sharma LP, Nilanchal Patel, Ghose MK, & Debnath P (2013). Synergistic application
434 of fuzzy logic and geo-informatics for landslide vulnerability zonation—a case study in
435 Sikkim Himalayas, India. *Appl Geomat* 5:271-284

436 Solaimani K, Mousav SZ, & Kavian A (2013). Landslide susceptibility mapping based
437 on frequency ratio and logistic regression models. *Arabian Journal of Geosciences*, 6(7),
438 2557-2569

439 Sujatha ER, Rajamanickam V, Kumaravel P, Saranathan E (2013). Landslide
440 susceptibility analysis using probabilistic likelihood ratio model—a geospatial-based
441 study. *Arab J Geosci* 6(2):429–440

442 Tien Bui, D., Pradhan, B., Lofman, O., Revhaug, I., and Dick, O.B., (2012). Spatial
443 prediction of landslide hazards in Hoa Binh province (Vietnam): a comparative
444 assessment of the efficacy of evidential belief functions and fuzzy logic models. *Catena*,
445 96, 28–40.

446 Tien Bui, D., Pradhan, B., Revhaug, I., Nguyen, D.B., Pham, H.V., and Bui, Q.N.,
447 (2013). A novel hybrid evidential belief functionbased fuzzy logic model in spatial
448 prediction of rainfall-induced shallow landslides in the Lang Son city area (Vietnam).
449 *Geomatics Natural Hazards & Risk*, doi:10.1080/19475705.2013.843206.

450 Ulusay, R., Aydan, Ö., and Kılıç, R., (2007). Geotechnical Assessment of the 2005
451 Kuzulu landslide (Turkey). *Engineering Geology*, 89 (1), 112-128.

452 Vahidnia, M.H., Alesheikh, A.A., Alimohammadi, A., Hosseinali, F., (2010). A GIS-
453 based neurofuzzy procedure for integrating knowledge and data in landslide
454 susceptibility mapping. *Computers and Geosciences* 36 (9), 1101–1114.

455 Van Westen CJ, Lulie GF (2003). Analyzing the evolution of the Tessina landslide
456 using aerial photographs and digital elevation models. *Geomorphology* 54(1–2):77–89

457 Wu Y., Li W., Liu P., Bai H., Wang Q., He J., Liu Y., Sun S. 2016, Application of
458 analytic hierarchy process model for landslide susceptibility mapping in the Gangu
459 County, Gansu Province, China. *Environ Earth Sci* (2016) 75:422 DOI 10.1007/s12665-
460 015-5194-9

461 Xu, C., Dai, F.C., Xu, X.W., and Lee, Y.H., (2012a), GIS-based support vector
462 machine modeling of earthquake-triggered landslide susceptibility in the Jianjiang
463 River watershed, China. *Geomorphology*, 145–146, 70–80.



464 Xu, C., Xu, X.W., Dai, F.C., and Saraf, A.K., (2012b). Comparison of different models
465 for susceptibility mapping of earthquake triggered landslides related with the 2008
466 Wenchuan earthquake in China. *Computers & Geosciences*, 46, 317–329.

467 Yalcin A. and Bulut F. (2007). Landslide susceptibility mapping using GIS and digital
468 photogrammetric techniques: a case study from Ardesen (NE-Turkey), *Natural Hazards*,
469 vol. 41, no. 1, pp. 201-226

470 Yalcin A., (2008). GIS-based landslide susceptibility mapping using analytical
471 hierarchy process and bivariate statistics in Anderson (Turkey): comparision of results
472 and confirmations, *Catena*, vol. 72, no. 1, pp. 1-12.

473 Yalcin, A., Reis, S., Aydinoglu, A.C., Yomralioglu, T., (2011). A GIS-based
474 comparative study of frequency ratio, analytical hierarchy process, bivariate statistics
475 and logistics regression methods for landslide susceptibility mapping in Trabzon, NE
476 Turkey. *Catena* 85: 274–287.

477 Yilmaz I., (2009a). Landslide susceptibility using frequency ratio, logistic regression,
478 artificial neural networks and their comparison: a case study from Kat landslides
479 (Tokat-Turkey). *Comput Geosci* 35(6):1125–1138

480 Yilmaz, I., (2010). Comparison of landslide susceptibility mapping methodologies for
481 Koyulhisar, Turkey: conditional probability, logistic regression, artificial neural
482 networks, and support vector machine. *Environmental Earth Sciences*

483 Yilmaz, I. and Keskin, I. (2009). GIS based statistical and physical approaches to
484 landslide susceptibility mapping (Şebinkarahisar, Turkey). *Bullettin of Engineering
485 Geology and Environment*, 68:4; 459-471.

486 Youssef, A.M., Pradhan, B., and Gaber, A.F.D., and Buchroithner, M.F., (2009).
487 Geomorphological Hazards Analysis along The Egyptian Red Sea Coast between
488 Safaga and Quseir. *Natural Hazards & Earth System Sciences*, 9, 751–766.

489 Youssef, A.M., Pradhan, B., and Maerz, H.N., (2013). Debris flow impact assessment
490 caused by 14 April 2012 rainfall along the Al- Hada Highway, Kingdom of Saudi
491 Arabia using high-resolution satellite imagery. *Arabian Journal of Geosciences*, DOI:
492 10.1007/s12517-013-0935-0.

493 Youssef, A.M., Al-Kathery M., Pradhan, B.,(2015). Landslide susceptibility mapping at
494 Al-Hasher Area, Jizan (Saudi Arabia) using GIS-based frequency ratio and index of
495 entropy models *Geosciences Journal* Vol. 19, No. 1, p. 113 – 134.

496 Yufeng, S., Fengxiang, J., (2009). Landslide Stability Analysis Based on Generalized
497 Information Entropy. 2009 International Conference on Environmental Science and
498 Information Application Technology, pp. 83–85